Eur. Phys. J. B **37**, 117–125 (2004)
DOI: 10.1140/epjb/e2004-00036-x

THE EUROPEAN PHYSICAL JOURNAL B

Quantitative interpretation of EELS and REELS spectra

V. Afanas'ev, A. Lubenchenko[a], and M. Gubkin

General Phys. and Fusion Department, Moscow Power Engineering Institute, Krasnokazarmennaya 14, Moscow, Russia

Received 15 July 2003 / Received in final form 9 October 2003
Published online 19 February 2004 –

Abstract. A critical analysis of the present day Electron Energy Loss Spectroscopy (EELS) data interpretation methods has been done. The necessity for the consideration of a target as a multilayered structure with different inelastic energy loss cross sections in the surface and the bulk layers has been shown to be a reality both for the transmission EELS and the reflection EELS (REELS). A method to reconstruct inelastic energy loss cross sections in various target layers from the experimental data has been presented. Essential qualitative and quantitative dependence of the path length distribution function for reflected electrons as a function of scattering angle has been revealed. The tested method for extraction of the information from REELS experiments with angular resolution has been presented.

PACS. 34.80.-i Electron scattering – 34.50.Bw Energy loss and stopping power – 25.30.Fj Inelastic electron scattering to continuum

1 Introduction

EELS spectra provide detailed information on the target under study. The energy loss in both transmission and reflection experiments is due to the multiple interactions with the target atoms [1]. The development of the method of extracting the electron differential inelastic scattering cross-section $\omega_{in}(E_0, \Delta)$ (E_0 – probing beam energy, Δ – energy loss) from the experimental data is one of the most topical issues in quantitative EELS [2,3]. Using a small-angle approximation one can write down the spectrum of electrons reflected from a target in the form of a convolution:

$$R(d, \Delta, \Omega_0, \Omega) = \int_0^\infty A_R(x, d, \Omega_0, \Omega)\, T_{in}(x, \Delta)\; dx \quad (1)$$

$$T(d, \Delta, \Omega_0, \Omega) = \int_0^\infty A_T(x, d, \Omega_0, \Omega)\, T_{in}(x, \Delta)\; dx, \quad (2)$$

where equation (1) is for the reflected electrons and (2) for the electrons transmitted through the target. Here $A_{R,T}(x, d, \Omega_0, \Omega)$ are path distribution functions of the electrons reflected [3,4] from the plane-parallel target or transmitted through the target [5], where x – path length, d – target thickness, $\Omega_0 = \{\theta_0, \varphi_0\}$, $\Omega = \{\theta, \varphi\}$ – the solid angles corresponding to the electrons entering and leaving the layer respectively, and $T_{in}(x, \Delta)$ – the general Landau solution [6] describing the energy loss spectrum of the electrons that took path x. A detailed description of the methods to calculate $T_{in}(x, \Delta)$ for the case of uniform layers is given in [5].

One of the purposes of the present paper is to generalize the results [3,7] for the case of multilayer non-homogeneous targets. Transmission EELS experiments [7] correspond to the case where the target thickness d is of the order of the average inelastic scattering length l_{in} and the probing beam energy E_0 varying from tens to hundreds keV. For the probing beam parameters given in [7,8] the electron transport path in the solid is essentially greater than the scattering length in the inelastic channel $l_{tr} \gg l_{in}$ and passing through the target does not result in any important isotropization of the beam. Therefore expression (2) $A_T(x, d, \Omega_0, \Omega)$ can be written as

$$A_T(x, d, \Omega_0, \Omega) = \delta(x - d/\mu_0)\, \delta(\Omega_0 - \Omega),$$

where $\delta(x)$ is Dirac function and μ_0 – the cosine of angle between surface normal and incident beam. Consequently, the approach for reconstructing $\omega_{in}(E_0, \Delta)$ based on the Landau solution [6] is sufficient for interpreting transmission EELS spectra provided the difference in inelastic cross sections for various layers is taken into account.

A detailed and reliable solution of the elastic problem is of major importance for REELS. The influence of the reflected electrons path distribution function $A_R(x, d, \Omega_0, \Omega)$ on the shape of the extracted $\omega_{in}(E_0, \Delta)$ is analyzed in [2,3] where a strong qualitative dependence of the extracted cross section shape on the $A_R(x, \infty, \Omega_0, \Omega)$ parameters is noted. It should also be noted that the assumptions used to determine the function $A_R(x, \infty, \Omega_0, \Omega)$ in [4] (let us write it as $A_R^\infty(x, \Omega_0, \Omega)$)

[a] e-mail: lub@phns.mpei.ac.ru

provide a reliable description for the paths with $x > \alpha\, l_{tr}$, $\alpha \simeq 1$. A more detailed analysis employing a discrete flux approach with a larger number of scattering directions of the elementary scattering act will enable us to expand the x range (i.e. to decrease α) where the function $A_R^{\infty}(x, \Omega_0, \Omega)$ is reliably identified. At $x \to 0$ the path distribution function is determined by low-multiplicity scattering processes in the elastic channel and therefore a detailed description of the elastic scattering cross section $\omega_{el}(E_0, \gamma)$ is needed (γ – is the electron scattering angle between the Ω and Ω_0 directions). This cannot be provided by the discrete flux approach [3].

At present one can give a most detailed description of $A_R(x, d, \Omega_0, \Omega)$ for the needs of REELS by solving the boundary-value problem for the transport equation using the invariant imbedding approach [9,10]; after the linearization procedure one can obtain an analytical solution in the form of a Legendre polynomial series [9,10]. This approach provides an adequate description of $A_R(x, d, \Omega_0, \Omega)$ within the x range $0 < x < l_{tr}$ and an exact description of the low-multiplicity scattering contribution to $A_R(x, d, \Omega_0, \Omega)$. The development of REELS with angle resolution necessitates the investigation of $A_R(x, d, \Omega_0, \Omega)$ with high accuracy.

2 The interpretation of the transmission EELS spectra in the framework of the multilayer model

The difference in electron excitation spectra in the surface and in the bulk layers leads us to interpret transmission EELS spectra with upper and lower sub-layers in the plane-parallel layer under study. As the first approximation, let us restrict ourselves to a three-layer target model. Incident electrons excite surface plasmons in the top and the bottom layers (both having thickness d_s) and bulk plasmons in the intermediate layer with thickness d_b (we assume energy losses due to electron-hole transitions and ionization are the same throughout the target). Thus transmission function can be written as follows:

$$T_{in}(d_b, d_{s_1}, d_{s_2}, \Delta) = \int_0^{\Delta}\int_0^{\varepsilon} T_{in}^{s}(d_{s_1}, \Delta - \varepsilon) \times T_{in}^{b}(d_b, \varepsilon - \varepsilon')\, T_{in}^{s}(d_{s_2}, \varepsilon')\; d\varepsilon' d\varepsilon. \quad (3)$$

Subscript 1 corresponds to the upper layer and subscript 2 to the bottom layer. It is appropriate to mention here that the designations "top" and "bottom" for the case of transmission EELS are rather relative. To interpret the curve we use the approximation (see above) for which all the particles cover the same path, so taking into account the property of convolution (3) the geometry "top-bulk-bottom", "bottom-bulk-top", "bottom-top-bulk-top-bottom" etc. result in identical energy-loss spectra. To make the choice between these options one should analyze the angular distributions of the scattered electrons.

In a one-speed approximation the functions $T_{in}^{s}(d_s, \Delta)$ are the same for the top and the bottom layers, therefore equation (3) can be simplified:

$$T_{in}(d_b, d_s, \Delta) = \int_0^{\Delta} T_{in}^{s}(d_s, \Delta - \varepsilon)\, T_{in}^{b}(d_b, \varepsilon)\; d\varepsilon, \quad (4)$$

where $d_s = d_{s_1} + d_{s_2}$.

In real spectra, low-energy losses rarely happen to be described by a single frequency of surface plasmons attributed to the top and bottom layers of thickness d_s. This could be explained both by the developed surface morphology characteristic for the methods of thin film preparation and the influence of contaminations, oxide films, radiation-stimulated segregation etc. So the surface layers have to be divided into sub-layers d_{s_i} with the ith plasmon excitation energy ε_{pl_i} respectively.

The probability $P_{in}(\boldsymbol{q}, \Delta)$ for a charged particle with velocity v ($v = \sqrt{2E_0/m_e}$, m_e is electron mass), to create an electron gas excitation (that is, a bulk plasmon or electron-hole pair; for the detailed treatment of the surface excitations see for example [12,13]) with energy Δ and momentum $\mathbf{q}$ of unit length of transmission can be expressed as follows [14]:

$$P_{in}(\mathbf{q}, \Delta) = \frac{A}{v}\mathrm{Im}\left\{-\frac{1}{\epsilon(\boldsymbol{q}, \Delta)}\right\}\frac{\delta(\Delta - \boldsymbol{q}\boldsymbol{v})}{q^2}, \quad (5)$$

where A is a constant and $\epsilon(\mathbf{q}, \Delta)$ is the frequency- and wave vector-dependent dielectric constant of the electron gas. There are various approximations of $\epsilon(\mathbf{q}, \Delta)$ for the region of interest, one of them is [15]:

$$\epsilon(\mathbf{q}, \Delta) = 1 - \frac{\varepsilon_{pl}^2}{\Delta^2 - \beta^2 q^2 - q^4/4 + i\delta\Delta}, \quad (6)$$

where $\varepsilon_{pl}/\hbar$ is the plasma frequency ($\hbar$ – Planck constant), the constant β can be determined by fitting to a plasmon dispersion curve and δ is the damping constant which in the plasmon region (low q) is assumed to be small. Expression (6) is a suitable approximation not only for plasmon excitation but also for the creation of electron-hole pairs with high q. Making the substitutions $q^2 = q_{\perp}^2 + q_{\parallel}^2$, $q_{\perp} = m_e v\,\theta$, $q_{\parallel} = \Delta/v$ [14], $\mathbf{q}\,\mathbf{v} = q_{\parallel}\, v$ one can integrate over Ω to obtain the inelastic energy-loss differential cross-section $\omega_{in}(E_0, \Delta)$ and normalize it to obtain $I_{in}(\Delta)$

$$I_{in}(\Delta) = \frac{\int P_{in}(\mathbf{q}, \Delta)\; d\Omega}{\iint P_{in}(\mathbf{q}, \Delta)\; d\Omega d\Delta}. \quad (7)$$

In this paper we approximate the result of the integration of (7) by

$$I_{in}(\Delta) = \lambda_p I_p(\Delta) + \sum_i \lambda_{ion}^{i}\, I_{ion}^{i}(\Delta), \quad (8)$$

where
$I_p(\Delta) = \frac{K}{\left(\Delta^2 - \varepsilon_{pl}^2\right)^2 + b^4}$, $K = \frac{\pi}{\sqrt{8\left(\varepsilon_{pl}^4 + b^4\right)\left(\sqrt{\varepsilon_{pl}^4 + b^4} - \varepsilon_{pl}^2\right)}}$;

$$I^i_{ion}(\Delta) = \begin{cases} 0, & \Delta < J_i \\ \frac{(1+a_i)J_i^{1+a_i}}{\Delta^{2+a_i}}, & \Delta \geq J_i \end{cases}; \lambda^i_{ion} = \sigma^i_{ion}/\sigma_{in},$$

and $\lambda_p = \sigma_p/\sigma_{in}$ – the probabilities of scattering via ionization and plasmon channels in each elementary act of inelastic scattering respectively; σ_p, σ^i_{ion} – the cross sections of plasmon inelastic scattering and the core-level ionization respectively; ε_{pl} – plasmon excitation energy; J_i – internal shell ionization threshold energy; b, α_i – are varied parameters. It should be noted that the term "plasmon excitation" here means all the losses for the excitation of valence electrons including the excitation of electron-hole pairs as well, so that $\sigma_p = \sigma_{eh} + \sigma_{pl}$ where σ_{pl}, σ_{eh} are the excitation cross sections of the plasmon and electron-hole pair, respectively.

Since the energy interval of interest for the transmission EELS is very narrow (typically up to 200 eV) and is detected with extremely high energy resolution (tenths of eV), the $T^{s,b}_{in}(d,\Delta)$ function can be calculated by its expansion into a series which corresponds to the multiplicity of the inelastic scatterings [5]. Let us use the general Landau solution:

$$T_{in}(d,\Delta) = \frac{1}{2\pi i}\int\limits_{\alpha-i\infty}^{\alpha+i\infty} \exp\left[p\Delta - \tau_{in}\left(1 - \overline{I_{in}(p)}\right)\right]\, dp, \tag{9}$$

where $\tau_{in} = d/l_{in}$ is a dimensionless path length obtained from the inelastic mean free paths $l_{in} = (n_0\,\sigma_{in})^{-1}$, σ_{in} is the inelastic scattering cross section, n_0 is the target atom concentration, $\overline{I_{in}(p)}$ is the Laplace-image of the inelastic indicatrix $I_{in}(\Delta)$ (normalized to the inelastic scattering cross section).

An expansion of $\exp\left[\tau_{in}\overline{I_{in}(p)}\right]$ in (9) in the form of a Taylor series combined with the convolution theorem gives:

$$T_{in}(d,\Delta) = \exp(-\tau_{in})\left(\delta(\Delta) + \sum_{k=1}^{\infty}\frac{\tau^k_{in}}{k!}I^{(k)}(\Delta)\right) \tag{10}$$

where $I^{(k)}(\Delta) = \int\limits_0^{\Delta} I^{(k-1)}(\Delta-\varepsilon)\, I^{(1)}(\varepsilon)\, d\varepsilon$, $I^{(1)}(\Delta) = I_{in}(\Delta)$.

When making specific calculations using formula (10) one should take into account that the ratio of the surface layer thickness d_s to the mean free path in the inelastic channel l_{in} is significantly less than unity: $\tau_s = d_s/l_{in} \ll 1$. It should be noted that the d_s value depends on the surface morphology and the surface contaminations. In this paper we consider d_s as a parameter characterizing the size of the d_s region having properties different to those in the bulk. The value of d_s will be determined by processing experimental data with the method under discussion.

Therefore a first order approximation of d_s can be written as

$$T^s_{in}(d_s,\Delta) = \exp(-\tau_s)\left(\delta(\Delta) + \tau_s\, I^s_{in}(\Delta)\right). \tag{11}$$

The inelastic indicatrix $I^s_{in}(\Delta)$ is described by (8) with parameters ε^s_{pl}, λ^s_{pl}, b_s corresponding to the frequencies and inelastic cross sections of the surface plasmons.

The function $T^b_{in}(d_b,\Delta)$ is determined from the series in (10) in which ten or more (depending on the width of experimental energy interval ΔE) terms have to be included.

The reconstruction of the cross section $\omega_{in}(E_0,\Delta)$ is based on the fitting-procedure: $\omega^0_{in}(E_0,\Delta)$ is taken from (8) with parameters from the tables in [16] as a zero approximation followed by the minimization of the functional

$$t = \int\limits_0^{\Delta E}\left(T^{\exp}_{in}(d,\Delta) - T_{in}(d,\Delta)\right)\, d\Delta \tag{12}$$

by means of varying the $T_{in}(d,\Delta)$ function parameters. Here $T^{\exp}_{in}(d,\Delta)$ is experimentally measured EELS spectrum. Finally $\omega_{in}(E_0,\Delta)$ is presented in the same form as in (8) with parameters reconstructed from the minimizing functional (12).

EELS spectra for 120 keV electrons transmitted through silicon (Si) and aluminum (Al) targets with a thickness of the order of 100 nm [7] are shown in Figure 1. Using the peak for elastically backscattered electrons from [7] one can unambiguously determine $\tau_{in} = d/l_{in}$. It is determined by the first term of (7). Figure 1 enables us to compare the function calculated from (5) (solid curve), the experimental data [7] for the case of multiple scatterings and the curve calculated taking into account the bulk excitations only (dotted line in Fig. 1). One can see that in the latter case the peak of the first-order scattering fits well but the discrepancies with the experimental curve grow for the the higher orders of scattering. Actually one can achieve a satisfactory agreement between the experimental and the calculated data by considering the target as the three-layer structure (Fig. 1) with layers having various thickness ($d = 289$ nm, $d_s = d_{s_1} + d_{s_2} = 17$ nm, $d_b = 272$ nm for silicon; $d = 148$ nm, $d_s = 11$ nm, $d_b = 137$ nm for aluminium) and by taking into account various plasma oscillation frequencies (Fig. 2). Single-scattering inelastic cross-sections $\omega_{in}(E_0,\Delta)$ in the bulk and in the surface layers are shown in Figure 2 on a logarithmic scale. Since the energy losses interval under discussion corresponds to $\Delta = 0 \div 70$ eV the ionization losses spectrum is not shown (the lowest ionization threshold of the L_3 shell of Si is equal to 104 eV, and the L_3 shell of Al =80 eV). The cross-section parameters corresponding to the EELS data for Si and Al at $E_0 = 120$ keV (8) are shown in Table 1.

In the course of experimental data interpretation and its comparison with the results of [7] transmission function $T^{\exp}_{in}(d,\Delta)$ was found to have a peculiar behavior which seems characteristic of both silicon and aluminum targets in the region of 4 eV (Fig. 1). We can explain this fact by assuming that the spread function of the energy-analyzer used in [7] is "two-humped" and does not follow Gaussian distribution.

An attempt to reconstruct a single-scattering inelastic cross-section $\omega_{in}(E_0,\Delta)$ from the multi-order

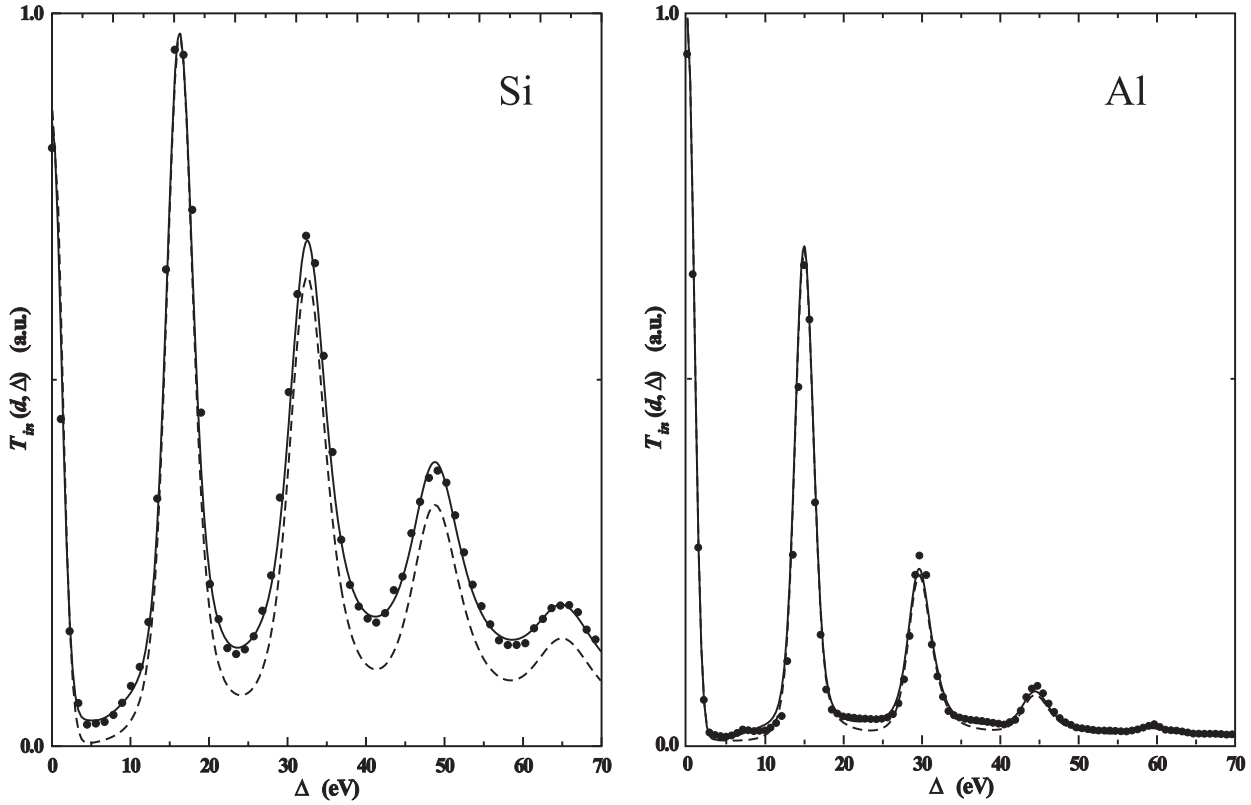

Fig. 1. EELS data for electrons of $E_0 = 120$ keV having passed through the silicon and aluminum films. Points – experiment [7], solid curve – calculations using cross-sections $\omega_{in}^{b}(\Delta)$, $\omega_{in}^{s_1}(\Delta)$, $\omega_{in}^{s_2}(\Delta)$ (see Fig. 2) carried out on the basis of the method developed in the present paper, dotted line – the curve calculated taking into account the bulk excitations only.

Table 1. Electron inelastic scattering cross-section parameters. Superscripts s_1, s_2 and b correspond to the top, the bottom and the bulk layer respectively.

Silicon	Aluminum
$\sigma_p^{s_1} + \sigma_p^{s_2} =$	
$\sigma_p^s = \sigma_p^b = 0,00014$ nm^2	$\sigma_p^s = \sigma_p^b = 0,00011$ nm^2
$\varepsilon_{pl}^{s_1} = 11,4$ eV; $b^{s_1} = 8,9$ eV	
$\varepsilon_{pl}^{s_2} = 4,1$ eV; $b^{s_2} = 3,9$ eV	$\varepsilon_{pl}^{s} = 10,5$ eV; $b^{s} = 9,8$ eV
$\varepsilon_{pl}^{b} = 16,4$ eV; $b^{b} = 6,7$ eV	$\varepsilon_{pl}^{b} = 14,8$ eV; $b^{s} = 4,2$ eV

scattering spectrum using a Fourier-logarithmic deconvolution method (it can be derived from the general Landau solution) was undertaken by Egerton and Wang [7]. In this work the authors neglected the differences between the inelastic cross-sections in the surface region and cross-sections in the bulk to simplify calculations. This approximation results in various peculiarities of the reconstructed function that have no physical meaning. The most striking of them is that in which $\omega_{in}(E_0, \Delta)$ has a negative value. Cross-sections extracted with the help of the technique under discussion are presented in Figure 2. For each of $\omega_{in}^{b}(\Delta)$, $\omega_{in}^{s_1}(\Delta)$, $\omega_{in}^{s_2}(\Delta)$ the region is marked where the specific energy-loss mechanism is valid. The cross-section $\omega_{in}^{b}(\Delta)$ (curve 3) is characteristic of the uniform region in the bulk; cross-sections $\omega_{in}^{s_1}(\Delta)$ (curve 1) and $\omega_{in}^{s_2}(\Delta)$ (curve 2) are valid in the near-surface layers. The cross-section extracted in [7] (curve 4) is presented for comparison.

3 REELS. Effect of the scattering angle on reflected electrons path distribution

Reflected electron energy loss spectroscopy (REELS) has various advantages in experimental performance as compared to transmission EELS. REELS provides principally new capabilities for the electron energies corresponding to the inelastic mean free path l_{in} of several mono-layers (transmission EELS is practically unfeasible in such case). However, as it is evident from equation (1) an adequate interpretation of REELS experiments requires a detailed quantitative description of the path distribution function $A_R(x, d, \Omega_0, \Omega)$ for short paths x. As the REELS reflection signal is formed on paths as long as $x \approx l_{in}$, and the typical inequality for the electron scattering is $l_{in} \ll l_{tr}$ [9], we arrive at $x \ll l_{tr}$ thus proving the small-angle approximation to be valid for the reflection EELS. A deduction of function $A_R(x, d, \Omega_0, \Omega)$ in [9] can be made using the boundary-value problem solution for

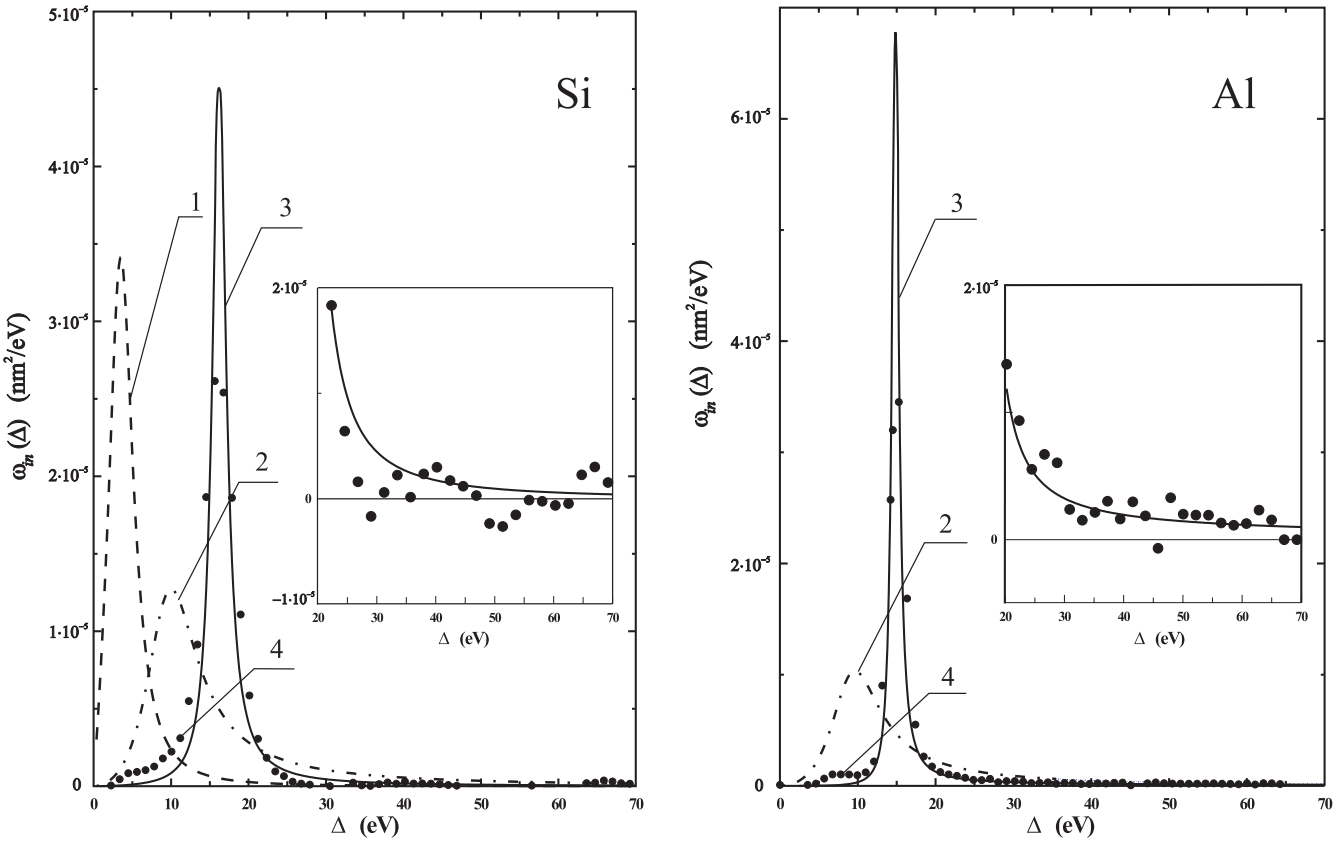

Fig. 2. Electron inelastic scattering cross-sections: 1) $\omega_{in}^{s1}(E_0, \Delta)$ – for the top layer, 2) $\omega_{in}^{s2}(E_0, \Delta)$ – for the bottom layer, 3) $\omega_{in}^{b}(E_0, \Delta)$ – for the bulk, 4) $\omega(E_0, \Delta)$ – calculated data from [7], insert: enlarged part of $\omega(E_0, \Delta)$ from [7].

the transfer equation by means of an invariant-imbedding approach. An analytical solution can be obtained with the small-angle approximation. According to [4,9] the function $A_R^{\infty}(x, \Omega_0, \Omega)$ is calculated as follows:

$$A_R^{\infty}(x, \Omega_0, \Omega) = n_0 \omega_{el}(\gamma) \exp(-n_0 \sigma_{el} x) + n_0 \sum_{l=1}^{\infty} \frac{2l+1}{2} (\omega_l - \sigma_{el}) P_l(\gamma) \times \left[\exp(-n_0(\omega_l - \sigma_{el})x) - \exp(-n_0 \sigma_{el} x)\right], \quad (13)$$

where ω_l are coefficients of the differential elastic scattering cross section $\omega_{el}(\gamma)$ after expansion into a Legendre polynomial $P_l(\gamma)$ series, σ_{el} is the full elastic scattering cross section, and n_0 is the concentration of target atoms. The behavior of the path length distribution function $A_R^{\infty}(x, \Omega_0, \Omega)$ at various scattering angles and probing beam energies E_0 can be unambiguously determined by function (13) which is an indubitable advantage if one compares it with the approach most used nowadays. In the latter approach: i) $A_R^{\infty}(x, \Omega_0, \Omega)$ is ambiguous, ii) the angle distributions of elastically scattered electrons and electrons having suffered multiple collisions are the same which is contrary to experimental data. The procedure used for the calculation of the function $A_R^{\infty}(x, \Omega_0, \Omega)$ gives a precision in the determination of the path distribution function at $x \to 0$ coinciding with the precision in the determination of the elastic cross-section $\omega_{el}(\gamma)$.

Substitution of (10) and (13) into equation (1) gives:

$$R(d, \Delta, \Omega_0, \Omega) = C_0(d, \Omega_0, \Omega)\, \delta(\Delta) + \sum_{k=1}^{\infty} C_k(d, \Omega_0, \Omega)\, I^{(k)}(\Delta), \quad (14)$$

where

$$C_k(d, \Omega_0, \Omega) = \int_0^{\infty} A_R(x, d, \Omega_0, \Omega) \frac{(x/l_{in})^k}{k!} \exp(-x/l_{in})\, dx \approx \int_0^{d(1/\mu_0 + 1/\mu)} A_R^{\infty}(x, \Omega_0, \Omega) \frac{(x/l_{in})^k}{k!} \exp(-x/l_{in})\, dx \quad (15)$$

where the coefficients of the reflection function expansion into a series of $I^{(k)}(\Delta)$ are similar to (10), $C_k(d, \Omega_0, \Omega)$ is the angular distributions of the elastically reflected electrons, and μ, μ_0 are the cosines of the angles between the surface normal and the reflected and the incident beams respectively.

A correlation between the calculated values of $C_0^{\infty}(\Omega_0, \Omega)$ and the experimental data obtained by Bronschtein and Pronin [17] for the angle distribution of elastically scattered electrons can be seen in Figure 3.

It is convenient to use a more detailed form of (14) in which the plasmon and ionization channels and the interference between them are considered in an explicit form:

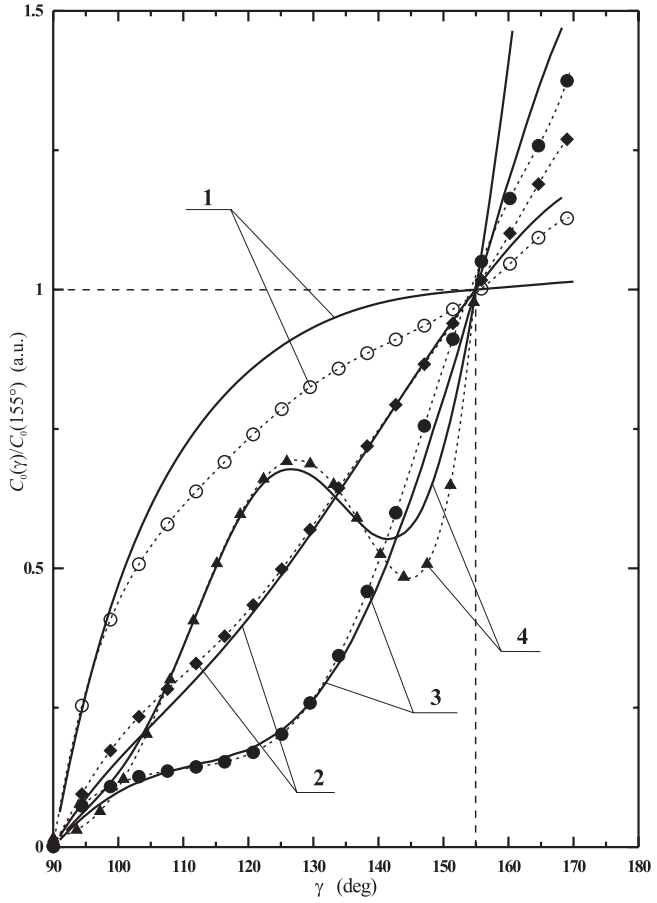

Fig. 3. Dependence of $C_0^{\infty}(\Omega,\Omega_0)$ on scattering angle γ. Initial electron energy $E_0 = 1$ keV. 1) target of Al, 2) target of Cu, 3) target of Ag, 4) target of Au. Solid line – calculation, doted line with points – experimental data [17].

$$R\left(d,\Delta,\Omega_0,\Omega\right) = C_0\left(d,\Omega_0,\Omega\right)\delta\left(\Delta\right) + \sum_{k=1}^{\infty}\left(\lambda_p\right)^k C_k\left(d,\Omega_0,\Omega\right) I_p^{(k)}\left(\Delta\right) + \sum_{k=1}^{\infty}\left(\lambda_i\right)^k C_k\left(d,\Omega_0,\Omega\right) I_i^{(k)}\left(\Delta\right) + \sum_{k=1}^{\infty}\sum_{n=1}^{\infty}\left(\lambda_i\right)^k\left(\lambda_p\right)^n \frac{n!k!}{(n+k)!} C_{k+n}\left(d,\Omega_0,\Omega\right) \times \int_0^{\Delta} I_i^{(k)}\left(\Delta-\varepsilon\right) I_p^{(n)}\left(\varepsilon\right) d\varepsilon. \quad (16)$$

To compare the results of our calculations with the experimental data a spread function of the energy analyzer $g\left(\Delta\right)$ was expressed as a Gaussian distribution with a half-width ξ that corresponds to the energy resolution of the experiments to be interpreted:

$$g\left(\Delta\right) = \frac{1}{\sqrt{2\pi}\xi}\exp\left(-\frac{\Delta^2}{2\xi^2}\right). \quad (17)$$

So the function R_g to be compared with experimental data is

$$R_g\left(d,\Delta,\Omega_0,\Omega\right) = \int_0^{E_0} g\left(\Delta-\varepsilon\right) R\left(d,\varepsilon,\Omega_0,\Omega\right)\, d\varepsilon \quad (18)$$

with $R\left(d,\Delta,\Omega_0,\Omega\right)$ determined by (16).

The method developed allows a simple generalization in the case of electron reflection from inhomogeneous layered structures. Let us consider the target consisting of multiple layers d_0, d_1,..., d_n (the subscript denotes the layer number) of different materials 0, 1, ..., n, where the numbering begins from the upper layer. Equation (14) in this case on account of the additivity of the integral takes the form:

$$R_{0,1,\ldots}\left(d_0,d_1,...,\Delta,\Omega_0,\Omega\right) = \sum_{i=0}^{n}\int_0^{d_i} A_{R_i}\left(d_0,d_1,...,x,\Omega_0,\Omega\right) T_{in_i}\left(x,\Delta\right)\, dx. \quad (19)$$

To describe the elastic channel in ith layer and inelastic scattering in ith layer the following designations have been introduced in equation (19):

$$A_{R_i}\left(d_0,d_1,...,x,\Omega_0,\Omega\right) = n_0\sum_{l=1}^{\infty}\frac{2l+1}{2}\left(\omega_{l,i}-\sigma_{el\ i}\right)P_l(\cos\gamma) \times\left[\exp\left(n_0\left(\omega_{l,i}-\sigma_{el\ i}\right)u + n_0\sum_{k=0}^{i-1}\left(\omega_{l,k}-\sigma_{el\ k}\right)u_k\right) - \exp\left(-n_0\,\sigma_{el\ i}\,u - n_0\sum_{k=0}^{i-1}\sigma_{el\ k}\,u_k\right)\right] + n_0\exp\left(-n_0\,\sigma_{el\ i}\,u - n_0\sum_{k=0}^{i-1}\sigma_{el\ k}\,d_k\right)\omega_{el}\left(\gamma\right), \quad (20)$$

$u = x\frac{\mu+\mu_0}{\mu\mu_0}$, $u_i = d_i\frac{\mu+\mu_0}{\mu\mu_0}$,

$$T_{in_i}\left(x,\Delta\right) = \frac{1}{2\pi j}\exp\left(-\tau-\sum_{k=0}^{i-1}\tau_k\right) \times\int_{\psi-j\infty}^{\psi+j\infty}\exp\left(p\Delta-\tau\overline{I_{in_i}(p)}-\sum_{k=0}^{i-1}\tau_k\overline{I_{in_k}(p)}\right)\, dp, \quad (21)$$

$\tau = \tau_{in}\frac{\mu+\mu_0}{\mu\mu_0}$, $\tau_i = \frac{d_i}{l_{in_i}}\frac{\mu+\mu_0}{\mu\mu_0}$.

For the case of the layer of material 0 on the semi-infinite substrate of material 1 we obtain:

$$R_{0,1}(d_0,\Delta,\Omega_0,\Omega) = R_0(d_0,\Delta,\Omega_0,\Omega) + \int_0^{\infty} A_{R_1}\left(\left(x+d_0\right)\frac{\mu+\mu_0}{\mu\mu_0},\Omega_0,\Omega\right) \times T_{in_1}\left(\left(x+d_0\right)\frac{\mu+\mu_0}{\mu\mu_0},\Delta\right)\, dx, \quad (22)$$

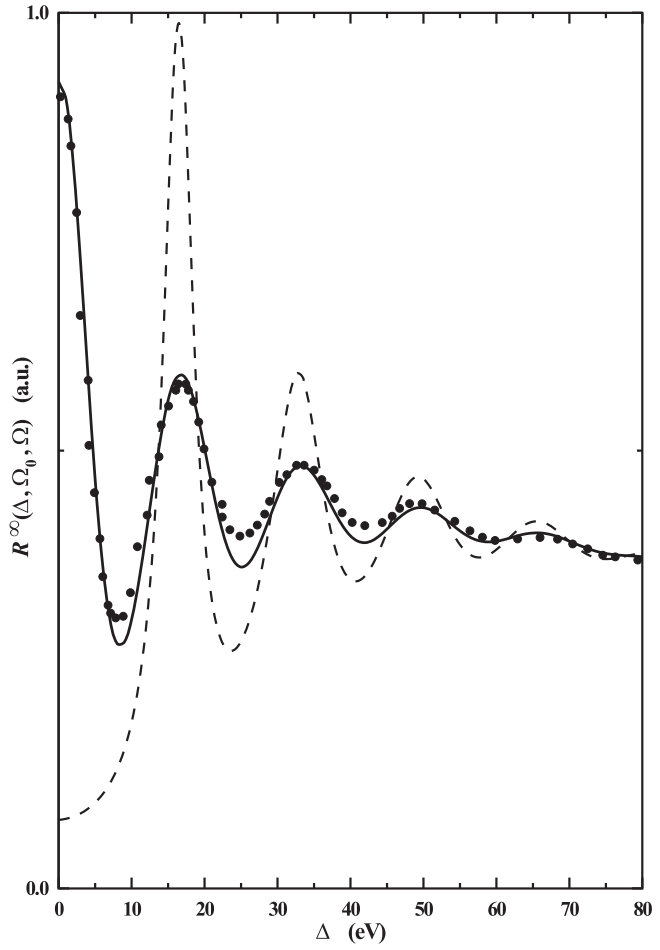

Fig. 4. REELS data for the electrons with $E_0 = 3116$ eV reflected from the polycrystalline specimen of Si at an angle of 138° (normal incidence of probing beam). Points – experiment [19], dotted line – calculation for the spectrometer with ideal resolution, solid curve – calculation taking into account real experimental resolution.

where $R_0(d_0, \Delta, \Omega_0, \Omega)$ is the reflection function corresponding to the layer of thickness d_0. Next taking into account (19, 20) and (21) we have

$$R_{0,1}(d_0, \Delta, \Omega_0, \Omega) = R_0(d_0, \Delta, \Omega_0, \Omega) + \int_0^{\Delta}\int T_{in_0}(d_0, \varepsilon, \Omega_0, \Omega')\, R_1^{\infty}(\Delta - \varepsilon, \Omega', \Omega)\; d\varepsilon d\Omega', \tag{23}$$

which is of the same form as the expression obtained in [18].

Figure 4 represents the spectrum of the electrons with $E_0 = 3116$ eV reflected at an angle of 138° (normal probing beam incidence) from a polycrystalline sample of Si. The narrowness of the energy region studied in experiments [19] does not allow an interpretation of the ionization energy losses. The low energy resolution of the experimental devices used in [19] resulted in the confluence of the bulk and the surface lines into one peak thus making it possible to treat the spectrum in Figure 4 within the framework of the uniform model with a single plasmon excitation frequency. The calculated curve is obtained using (14–18). To describe the REELS spectrum it is sufficient to use the first two terms in the right hand part of (16) which are responsible for the elastic peak and the excitation of plasmons:

$$R(\Delta, \Omega_0, \Omega) = C_0(\Omega_0, \Omega)\,\delta(\Delta) + \sum_{k=1}^{\infty}(\lambda_p)^k\, C_k(\Omega_0, \Omega)\, I_p^{(k)}(\Delta) \tag{24}$$

The experimental curve [19] corresponds to the narrow region of electron losses $0 < \Delta < J_i$ below the ionization threshold. The REELS spectrum is reconstructed on the basis of (24) for the semi-infinite media model and is represented in Figure 4 by a dashed line. If one approximates the spread function by a Gaussian distribution with a half-width $\xi = 3,9$ eV corresponding to the energy resolution of the experiments [19] in which $\Delta E/E_0 = 0,3\%$ and then makes the calculations using equation

$$R_g(\Delta, \Omega_0, \Omega) = C_0(\Omega_0, \Omega)\, g(\Delta) + \sum_{k=1}^{\infty}(\lambda_p)^k\, C_k(\Omega_0, \Omega)\int_0^{E_0} g(\Delta - \varepsilon) I_p^{(k)}(\varepsilon)\, d\varepsilon \tag{25}$$

the curve obtained (solid line in Fig. 4) fits well the experimental data. Contrary to the EELS data processing methods, the calculation technique presented here is based on the solution of the direct (not the reverse) problem and thus does not require an "elastic peak subtraction" procedure which can prove ambiguous. The coincidence of the calculated curve and the experimental one (Fig. 4) takes place at the following values of the parameters used: $\varepsilon_{pl} = 16,4$ eV, $b = 9$ eV, $l_{pl} = 7,9$ nm, $l_{in} = 5,4$ nm. It should be noted that for the first approximation, electron scattering parameters from [19] have been used; further refinement of them has been carried out on the basis of the fitting procedure.

A characteristic feature of the Al REELS spectrum obtained contrast to that obtained in [19] with high energy resolution is the presence of a clearly defined surface plasmon [20]. The interpretation of the experimental data represented in [20] should be carried out on the basis of a two-layer problem (23) in which the path distribution function is determined from the elastic problem solution for a uniform semi-infinite media. For the inelastic channel description the upper layer of thickness d_s should be marked; the value of $I_{in}^s(\Delta)$ for this layer in equations (21–23) describes the surface plasmon only where as the region below d_s is described by the cross-section (8)

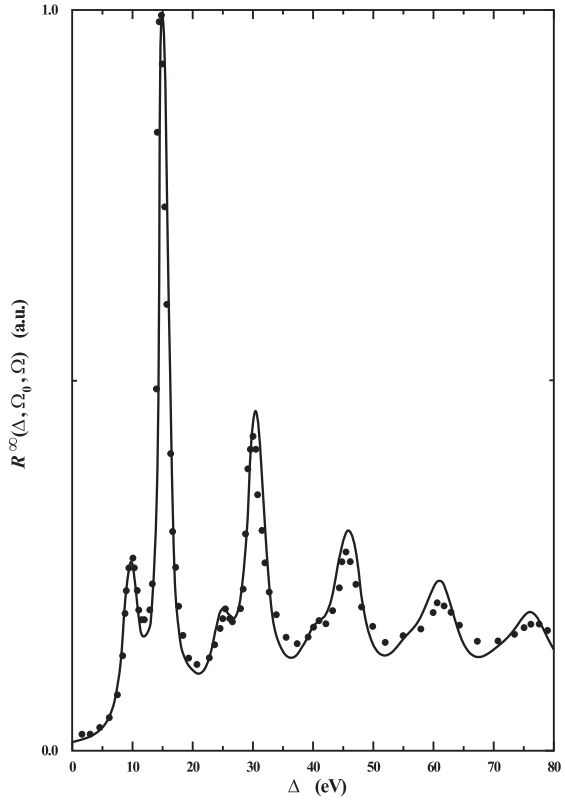

Fig. 5. REELS data for electrons with $E_0 = 2000$ eV reflected from the polycrystal specimen of Al at angle 155°. Points – experiment [20], solid curve – calculation in which two layered model separating regions of the bulk and the surface plasmons was used.

in which only the bulk plasmon $I^b_{in}(\Delta)$ is included:

$$R_{s,b}(d_s, \Delta, \Omega_0, \Omega) = R_s(d_s, \Delta, \Omega_0, \Omega) + \int_0^{\Delta} T^b_{in}\left(d_s \frac{\mu+\mu_0}{\mu\mu_0}, \varepsilon\right) \int_0^{\infty} A^b_R\left(x\frac{\mu+\mu_0}{\mu\mu_0}, \Omega_0, \Omega\right) \times T^b_{in}\left(x\frac{\mu+\mu_0}{\mu\mu_0}, \Delta-\varepsilon\right) dx d\varepsilon = R_s(d_s, \Delta, \Omega_0, \Omega) + \int_0^{\Delta} T^s_{in}\left(d_s\frac{\mu+\mu_0}{\mu\mu_0}, \varepsilon\right) \times R^{\infty}_b(\Delta-\varepsilon, \Omega_0, \Omega)\, d\varepsilon. \quad (26)$$

The first term in the right hand part of (26) determines the electron flux reflected from the upper layer of thickness d_s and can be calculated by means of expressions (20) and (21) where $I^s_{in}(\Delta)$ is determined by the surface plasmon parameters. The second term is the convolution of the inelastic transmission function (calculated using (9) with $I^s_{in}(\Delta)$) and the reflection function for a semi-infinite sample in which there exist only the losses caused by the bulk plasmon excitation and ionization. The calculation of R_s and R_b was carried out with the same path distribution A_R. The layer thickness d_s is of the order of several lattice parameters and should be treated as a fitting parameter since its value depends on a number of undefined factors mainly related to the surface morphology, the presence of oxides and contaminations. REELS spectra for the electrons reflected from Al with initial energy $E_0 = 2$ keV are shown in Figure 5. The solid line illustrates calculations based on the two-layer model (26) with the following parameters: $\varepsilon^b_{pl} = 15,3$ eV, $b^b = 5,9$ eV, $l^b_{pl} = 4,7$ nm, $\varepsilon^s_{pl} = 9,7$ eV, $b^s = 4,7$ eV, $l^s_{pl} = 4$ nm, $l^s_{in} = 3,8$ nm, $d_s = 1,1$ nm.

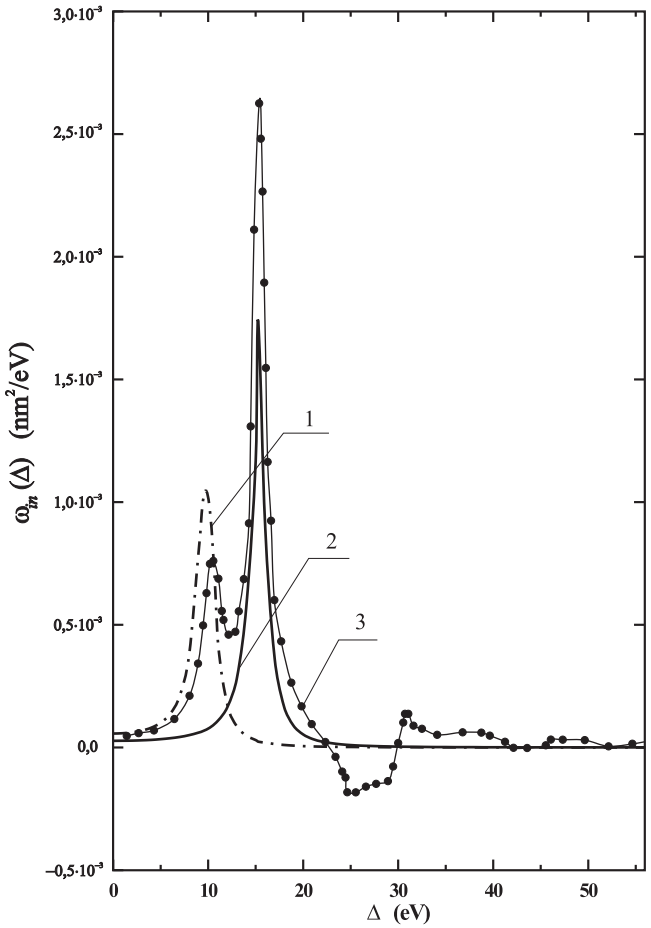

Fig. 6. Electron inelastic scattering cross-sections. 1) $\omega^s_{in}(E_0, \Delta)$ – for surface layer, 2) $\omega^b_{in}(E_0, \Delta)$ – for the bulk, 3) $\omega_{in}(E_0, \Delta)$ – calculated data from [20].

The inadequacy of the uniform model (not the two-layer model) can be seen from the following speculation: following the reasoning in [3,20] one uses the cross-section $I_{in}(\Delta) = \lambda_p I_p(\Delta) + \lambda_i I_i(\Delta)$ where in turn $I_p(\Delta) = \lambda^s_p I^s_p(\Delta) + \lambda^b_p I^b_p(\Delta)$ for the entire sample one will obtain a curve which has a clearly observable and overrated contribution from the many-order scattering of the s-plasmon and a "hole" of negative values which should appear in $I_{in}(\Delta)$. This is shown in Figure 6 and can be seen in papers [3,20].

4 Conclusion

We have compared different solid state diagnostics methods based on transmission and reflection EELS for the same material.

As the thicknesses mentioned above are the fitting parameters depending on the surface morphology, their values are determined by the minimization of the functional (12). The analysis carried out in the present paper shows that from the point of view of the EELS spectra interpretation a film and a semi-infinite sample are widely different from one another.

The most striking differences are observed inside the layers d_s where the surface plasmon excitation losses take place; the value of d_s^T extracted from the transmission experiments is several times higher than d_s^R extracted from the reflection experiments. The fact that the absolute values of d_s^T are of the order of tens mono-layers indicates the poor quality of the targets. The method of reconstructing d_s^T enables one to interpret its value as the size of the region in which the target properties are different from those of the uniform material far from the surface. The value of d_s^T is determined both by the developed surface morphology and by the contaminations which are impossible to remove. This fact signifies that the errors of the EELS target investigation method are fundamentally irremovable.

The REELS method, which permits the cleaning of targets in a vacuum chamber, provides much more reliable and unambiguous experimental data. This is confirmed by the fact that the depth of the near-surface region is of the order of several mono-layers. The complication of experimental data treatment method due to the problem of determining the path distribution function can be successfully surmounted which is demonstrated in the present paper.

References

1. H. Raerher *Excitation of Plamons and Interband Transitions by Electrons* (Springer, Berlin, 1979)
2. S. Tougard, P. Sigmund, Phys. Rev. B **25**, 4452 (1982)
3. S. Borodyansky, S. Tougard, Surf. Interface Anal. **23**, 689 (1995)
4. V.P. Afanas'ev, S.D. Fedorovich, A.V. Lubenchenko, A.A. Rysov, M.S. Esimov, Z. Phys. B **96**, 253 (1994)
5. V.P. Afanas'ev, A.V. Lubenchenko, A.A. Rysov, Surface Investigation. **12**, 1 (1996)
6. L.D. Landau, J. Phys. USSR. **8**, 201 (1944)
7. R.F. Egerton, Z.L.Wang, Ultramicroscopy **32**, 137 (1990)
8. L.A. Grunes, J.C. Barbour, L.S. Hung, J.M. Mayer, J.J. Ritsko, J. Appl. Phys. **56**, 168 (1984)
9. V.P. Afanas'ev *Fundamental processes and kinetics of high-temperature non-equilibrium plasma* (Edition MPEI, Moscow, 1988) (in Russian)
10. V.P. Afanas'ev, D. Naujoks, Phys. Stat. Sol. **164**, 133 (1991)
11. S. Tougard, I. Chorkendorf, Phys. Rev. B **35**, 6570 (1987)
12. A.A. Lucas, M. Sunjic, Phys. Rev. Lett. **26**, 229 (1971)
13. E. Evans, D.L. Mills, Phys. Rev. B **5**, 4126 (1972).
14. D. Pines, Ph. Nozieres *The Theory Of Quantum Liquids* (W.A. Bendjamin Inc., New York, Amsterdam, 1966)
15. B.I. Lundquist, Phys. Konderns. Mater. **6**, 206 (1967)
16. A.F. Akkerman *Simulation of trajectories of charged particles in medium* (Energoatomizdat, Moscow., 1991) (in Russian)
17. I. M. Bronschtein, V.P. Pronin, Sov. Phys.-Solid State. **29**, 2223 (1987)
18. V.P. Afanas'ev *High-energy electron flow reflection from layered solid structures. Collected articles on science 153* (Edition MPEI, Moscow, 1988) (in Russian)
19. G. Gergely, Surf. Interface Anal. **3**, 201 (1981)
20. S. Tougard, I. Chorkendorf, Phys. Rev. B **35**, 6570 (1987)